Journal of Applied Mechanics Vol. 4, pp. 145-152 (August 2001) JSCE

On the determination of ultrasonic waves emitted from transducers using laser measurements with applications to defect determination problems

レーザ計測によるトランスデューサの超音波波形決定とその欠陥決定問題への応用に関する考察

Hitoshi YOSHIKAWA* , Naoshi NISHIMURA** and Shoichi KOBAYASHI***
吉川仁・西村直志・小林昭一

*Student member, M. Eng., Dept. Global Environment Eng., Kyoto Univ.
(Yoshida-Honmachi, Sakyo-Ku, Kyoto 606-8501)
**Member, Dr. Eng., Assoc. Prof., Dept. Global Environment Eng., Kyoto Univ.
(Yoshida-Honmachi, Sakyo-Ku, Kyoto 606-8501)
***Fellow, Dr. Eng., Prof., Dept. Construction Eng., Fukui Univ. of Technology
(3-6-1 Gakuen, Fukui 910-8505)

An inverse problem of determining the elastic wave produced by an ultrasonic transducer from laser velocimetry data is considered. The quality of the inversion is tested via a comparison between experimental data and simulation results obtained with a 3 dimensional time domain elastodynamic BIEM using parallel computing. The agreements of these results are satisfactory. The feasibility of the determination of defects based on the laser measurements is also investigated. The size and location of an unknown defect are determined with high accuracy.

Key Words : *BIEM, inverse problem, ultrasonic transducer, laser interferometer, parallel computing*

1. Introduction

Determination of defects in structural members is one of fundamental issues of the non-destructive evaluation. In these few years, the present authors have been investigating the reconstruction of unknown defects from real data of ultrasound using a BIE (boundary integral equation) approach.[1),2),3)] As the data, the particle velocity associated with the ultrasound measured with a laser interferometer has been used. This is because the setting of the inverse problems assumes that one knows both incident elastic waves to illuminate the defects, and the scattered waves from the defects quantitatively.[4)] With the laser velocimetry one can measure the scattered waves quantitatively, but the incident waves still remain to be determined since these waves are generated by transducers with unknown characteristics. In view of this, an auxiliary inverse problem has been considered which uses real data obtained with a laser interferometer to determine the waves from the transducer[2)]. The quality of the inversion was then tested in a comparison between measured and calculated scattered waves from a known defect. The comparison turned out to be good, but not completely satisfactory for carrying out the reconstruction of defects.

To improve the results, Yoshikawa et al.[3)] attempted to use a more realistic, but still simple, model for the transducer to determine the incident waves[3)]. This model removed the assumption of the uniform distribution of the equivalent force under the transducer made in the previous investigation[2)]. Also a parallel BIEM[3)] for 3 dimensional elastodynamics in time domain was used to verify the result of the inversion, thus eliminating possible inaccuracy of the numerical solution caused by the coarse mesh. The comparison between measured and calculated scattered waves turned out not to be completely satisfactory, but the results were good enough for carrying out a preliminary reconstruction of defects. Indeed, a

simple inverse problem of determining the geometry of an unknown defect from real data was solved in Yoshikawa et al.[3] In this problem the radius and the depth of an unknown defect were determined numerically using the real ultrasound data. The estimated values were not very satisfactory (the estimated radius included an error of 20%), and further need for the improvement of the accuracy of the inversion was concluded.

In the present paper, we continue the efforts to improve the quality of the reconstructed incident waves from the transducer in order to improve the accuracy of the determination of unknown defects from ultrasonic data. Specifically, we reconsider the process of determining the equivalent load under the transducer, and attempt to identify the sources of error. We shall see that the setting of the experiment can be improved so that more information from the experiment can be taken into the analysis. Using the new experimental setting we shall carry out both experiments and inverse analysis to reconstruct the incident wave from the transducer. The comparison between the reconstructed incident wave from the transducer and the corresponding experimental results will be seen to be quite satisfactory. Finally, we shall see that a considerably improved reconstruction results are obtained in the inverse problem of determining the unknown defects using the new experimental setting.

2. Experiment and Inversion in Yoshikawa et al.[3]

We shall describe the experiment and the inversion discussed in the previous papers[2),3)] for the purpose of referential convenience.

2.1 Experiment

The test piece shown in Fig.1 is made of aluminium alloy, and has a circular cylindrical shape with the diameter of 200mm and the hight of 49.8mm. This test piece has an artificial defect, i.e., a cylindrical hole having the diameter of 19.8mm and the depth of 44.4mm from the bottom. We set an ultrasonic transducer (SONIX, central frequency = 500 KHz, diameter = 14.5mm) at the indicated position (20mm from the centre of the test piece) using silicone grease as the couplant. The ultrasonic transducer is then excited with an electric pulse generated by a pulser (RITEC SP-801). We then use laser interferometer (ONO measuring instruments LV-1300) to measure normal velocities at points denoted by $L_{1\text{-}4}$ and R_1 in the same figure. The points $L_{1\text{-}4}$ are taken 5mm apart from each other, and the points L_1 and R_1 are placed 22mm away from the centre of the transducer(the origin of the coordinate system).

The frequency range of the laser interferometer is from 1Hz to 2.5MHz. The interferometer produces a voltage proportional to the measured normal velocity, and the output from the interferometer is recorded with a digital oscilloscope (LeCroy 9384TM). The S/N ratio of the output is enhanced with a stacking of 5000 sweeps. In this experiment we determine the incident waves from the transducer by using the data obtained at $L_{1\text{-}4}$ in an interval of t where the responses at these points are not affected by the artificial defect. Our interest is to see if the incident waves thus reconstructed predicts the responses at the point R_1 sufficiently accurately that one can use the reconstruction result for the incident wave in the second inversion of determining the geometry of defects.

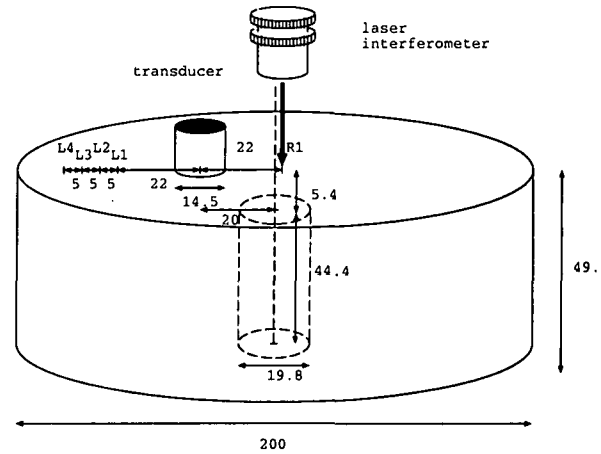

Fig. 1 Test piece. (unit: mm)

2.2 Determination of Equivalent Loads

(1) Formulation

One may model the action of the transducer to the test piece by a few time varying uniform normal loads $p_j(t)$ $(j = 1, \ldots, M)$ called equivalent loads. With this assumption one obtains a system of integral equa-

tions given by

$$V^i(t) = \sum_j^M \int_0^t k_j^i(t-s)\dot{p}_j(s)ds, \quad (i=1,\ldots,N) \quad (1)$$

where $k_j^i(t)$ is the normal displacement at the point x^i produced by the jth uniform load having a Dirac delta time variation, $V^i(t)$ is the normal velocity at x^i obtained with laser velocimetry, and N is the number of the experiments. The union of the area of application of the load p_j denoted by ∂D_{t_j} coincides with the area under the transducer.

Since this system of over determined integral equations of the first kind is unstable to solve numerically, we convert it into the following stabilised integral equations with the help of Tikhonov's regularisation[5]

$$\varepsilon\dot{p}_j(t) + \int_0^T K_{j\ell}(t,\tau)\dot{p}_\ell(\tau)d\tau = \sum_i \int_t^T k_j^i(s-t)V^i(s)ds, \quad (2)$$

$$K_{j\ell}(t,\tau) = \sum_i \int_{\max(t,\tau)}^T k_j^i(s-t)\ k_\ell^i(s-\tau)ds,$$

where ε is the Tikhonov parameter. The solution $\dot{p}_j$ of Eq. (2) then determines the elastic waves from the transducer as one solves a direct problem with this $\dot{p}_j$ as part of the boundary conditions. Namely, one solves the following initial boundary value problem for the unknown velocity $\boldsymbol{v}$:

$$\mu\Delta\boldsymbol{v} + (\lambda+\mu)\nabla\nabla\cdot\boldsymbol{v} = \rho\ddot{\boldsymbol{v}} \ \text{ in } D\times(t>0), \quad (3)$$
$$\mathrm{T}\boldsymbol{v} = 0 \ \text{ on } (\partial D \setminus (\partial D_{t_1}\cup\cdots\cup\partial D_{t_M}))\times(t>0),$$
$$\mathrm{T}\boldsymbol{v} = -\dot{p}_j(t)\boldsymbol{n} \text{ on } \partial D_{t_j}\times(t>0),$$
$$\boldsymbol{v}|_{t=0} = \dot{\boldsymbol{v}}|_{t=0} = 0 \ \text{ in } D,$$

where D is the domain under consideration, ∂D is the boundary of D, $\boldsymbol{n}$ is the unit normal vector to ∂D and T is the traction operator, respectively. The boundary integral equation for Eq. (3) is given by

$$\frac{1}{2}v_i(\boldsymbol{y},t) = \int_{\partial D}\int_0^t \Gamma_{ij}(\boldsymbol{y}-\boldsymbol{x},t-s)\mathrm{T}_{j\ell}v_\ell(\boldsymbol{x},s)dsdS - \barint_{\partial D}\int_0^t \Gamma_{Iij}(\boldsymbol{y},\boldsymbol{x},t-s)v_j(\boldsymbol{x},s)dsdS, \quad \boldsymbol{y}\in\partial D \quad (4)$$

where the integration sign with a superimposed $-$ stands for a Cauchy's principal value. The function Γ_{ij} is the fundamental solution for 3 dimensional elastodynamics and Γ_{Iij} is the double layer kernel defined, respectively, by

$$\Gamma_{ij}(\boldsymbol{x},t) = \frac{1}{4\pi\mu}\left[\frac{\delta(t-|\boldsymbol{x}|/c_T)}{|\boldsymbol{x}|}\delta_{ij} - c_T^2\frac{\partial}{\partial x_i}\frac{\partial}{\partial x_j}\left(\frac{(t-|\boldsymbol{x}|/c_T)_+}{|\boldsymbol{x}|} - \frac{(t-|\boldsymbol{x}|/c_L)_+}{|\boldsymbol{x}|}\right)\right], \quad (5)$$

$$\Gamma_{Iij}(\boldsymbol{y},\boldsymbol{x},t) = (\lambda\Gamma_{im,m}(\boldsymbol{y}-\boldsymbol{x},t)\delta_{jk} + \mu(\Gamma_{ij,k}(\boldsymbol{y}-\boldsymbol{x},t)+\Gamma_{ik,j}(\boldsymbol{y}-\boldsymbol{x},t))n_k(\boldsymbol{x}), \quad (6)$$

where ',$_j$' stands for $\partial/\partial x_j$, δ_{ij} is Kronecker's delta, x_+ is defined by $(x+|x|)/2$, c_L is the velocity of the P wave and c_T is the velocity of the S wave, respectively. The normal velocity at R_1 shown in Fig.1 is computed numerically from Eq. (4).

2.3 Results

Yoshikawa et al.[3] have carried out an inversion to determine $\dot{p}_j(t)$ using the velocities $V^i(t)$ $(i=1,\ldots,4)$ obtained at $L_{1\text{-}4}$ shown in Fig.1. The data in the interval of $t_0 \le t \le t_1$ are used in the inversion, where t_0 is the rise time at L_1, $t_1 = t_0 + T$ and $T = 6$ (μs). The action of the transducer is modelled by two equivalent loads, i.e., one (p_1) distributed on the circular area (∂D_{t_1}) under the oscillator of the transducer, and the other (p_2) on the rest of the area (∂D_{t_2}) under the transducer, respectively (Fig.2). One may then assume the domain for the analysis to be a half space since the reflection from the side and the bottom of the test piece is negligible. Hence one may use the well-known solution by Lamb[6] to obtain $k_j^i(t)$ in Eq. (1) and Eq. (2). The optimum Tikhonov parameter ε is obtained from the L-curve[7] to be 10^{-7}.

In this way Yoshikawa et al.[3] could determine the incident wave from the transducer. The computed and measured normal velocities at R_1 are shown in Fig.3. As we can see in this figure, the agreement of these results are satisfactory up to 7μs, but then the computed result shows a deviation from the curve of the measured results at around $t = 8\mu$s. Yoshikawa et al.[3] also presents a result of the same inverse problem of determining the shape of a defect as will be discussed later. They could, however, determine the radius of the defect only to within 20% of the true

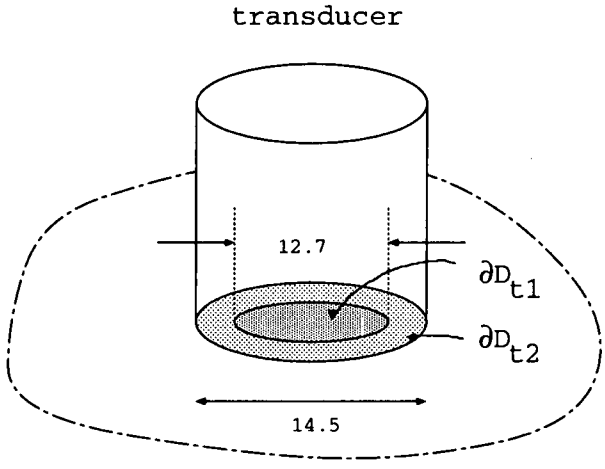

Fig. 2 Transducer. (unit: mm)

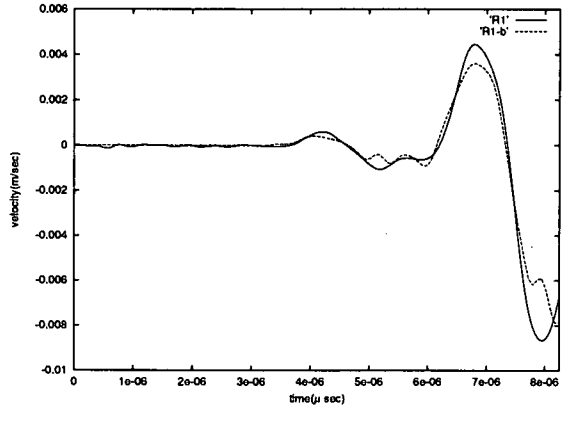

Fig. 3 Computed and measured normal velocity at R_1. R_1: measured, R_1-b: computed

value.

3. Criticism to the Earlier Investigation

As seen in the previous section the analysis in Yoshikawa et al.[3] was satisfactory to some extent, but not completely for carrying out the determination of defects. In this section we shall consider how one can improve the results in Yoshikawa et al.[3]

Fig.4 shows the behaviour of $\dot{p}$ as a function of time obtained using the method and data presented in Yoshikawa et al.[3] except that the distribution of $\dot{p}$ is assumed to be uniform under the transducer. The last assumption is introduced for the purpose of simplicity of the discussion. (See Yoshikawa et al.[3] for the plot of the $\dot{p}_j$ (2-DOF) used for obtaining the result in Fig.3. The 2-DOF results for $\dot{p}_j$ show the same behaviour as will be explained in Fig.4.) This figure shows an unnatural spiky behaviour at $t \approx 3\mu$s. We also see another, but much smaller, anomaly at $t \approx 1.5\mu$s. In the solution of Eq. (3) using this $\dot{p}$, the former anomaly begins to propagate from the edge of the transducer at $t \approx 3\mu$s and takes about 5μs to reach R_1 in the form of the Rayleigh wave, whose phase velocity is about 2900(m/s). Hence we expect to see the effect of this anomaly clearly at about 8μs at R_1, considering the fact that the most dominant carrier of wave motions in terms of the amplitude is the Rayleigh wave. This is in agreement with the observation made in Fig.3.

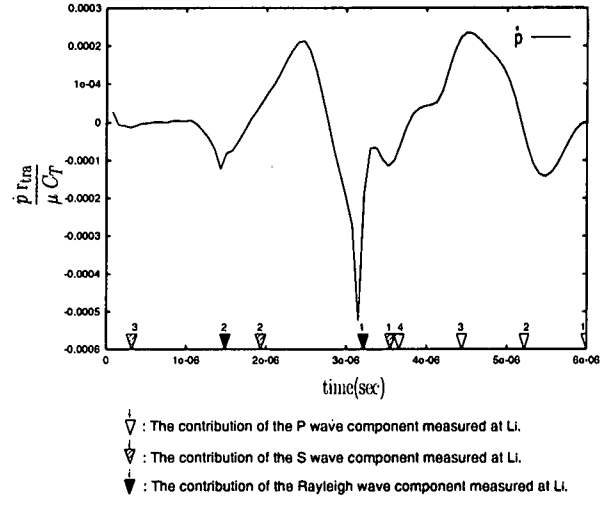

Fig. 4 Reconstructed pressure rate $\dot{p}$. r_{tra}: radius of the transducer

We now discuss why this anomaly takes place. The triangles in Fig.4 with a superposed number i show the arrival time of certain waves at the observation point L_i plotted backward from $t = T + t_0$ with $T = 6(\mu\mathrm{s})$, where t_0 is the rise time at L_1 and T is the period of the measurement. In the sequel we shall call the locations of these triangles 'backward arrival times'. It is easy to see that the information carried by a certain wave and observed at L_i is used in the determination of $\dot{p}$ in the interval of t between 0 and the relevant backward arrival time. Therefore the curve of $\dot{p}$ between the white triangle marked '2'($t \approx 5.2\mu$s) and 6μs is determined only from the information carried by P wave and observed at L_1, for example, and, therefore, may not be very reliable. It is seen that

the locations of the spikes correspond to the backward arrival times associated with the Rayleigh wave. In other words, we see anomalies at the instants when the amount of information of $\dot{p}$ carried by the Rayleigh wave changes suddenly. Judging from the curve in Fig.4, however, changes of the amount of information carried by other waves do not seem to contribute to the anomalous behaviour of $\dot{p}$. This observation may be explained from the facts that the biggest component of waves propagating on a surface is the Rayleigh wave and that a time variation of Lamb's solution is continuous at the arrival times of P and S waves and is discontinuous at the arrival time of Rayleigh's wave. Or, possibly, the difference between the assumed and true wave speeds of Rayleigh's wave may be responsible for this behaviour. At present, however, the authors do not have more definitive explanations for the occurrence of the anomalies.

To avoid the contamination of the solution by this anomaly, one may use the observation that the biggest anomaly is associated with the backward arrival time of the Rayleigh wave at the observation point closest to the transducer (L_1). Indeed, one may measure normal velocities $V^i(t)$ for longer periods of time $(0, T + \Delta T)$ and determine $\dot{p}$ in the same time interval using the technique presented previously, where $\Delta T > 0$. One then discards $\dot{p}$ for $t > T$ and takes the solution only in the time interval of $(0, T)$. Since the backward arrival time will then be delayed by ΔT, one may adjust ΔT so that one sees the contamination only after the particular time interval of interest.

Another observation to support the use of the elongated experimental data is the fact that the computed $\dot{p}$ in Fig.4 approaches zero as $t \to 6(\mu s)$. As a matter of fact, one shows easily that the solution to the integral equation in (2) approaches zero as $t \to T$ if $\epsilon > 0$ since the integrals on both sides of (2) vanish as $t \to T$. This means that we force $\dot{p}$ to vanish for $t \approx T$ in order to stabilise the solution of the integral equation. It is therefore obvious that it is desirable to take T larger than required in order to compute $\dot{p}$ accurately in the whole time interval of interest.

Fortunately, the experimental data used in Yoshikawa et al.[3] are available up to $7.5\mu s$. Utilising all the data in this interval, i.e. with $\Delta T = 1.5(\mu s)$, we could obtain the result for $\dot{p}$ shown by the solid line in Fig.5. Here again we have used a simplifying assumption that $\dot{p}$ stays uniform under the transducer. As is evident from this figure the anomaly at about $t = 3.2(\mu s)$ has been shifted to approximately $t = 4.7(\mu s)$. In Fig.6 we have compared the normal

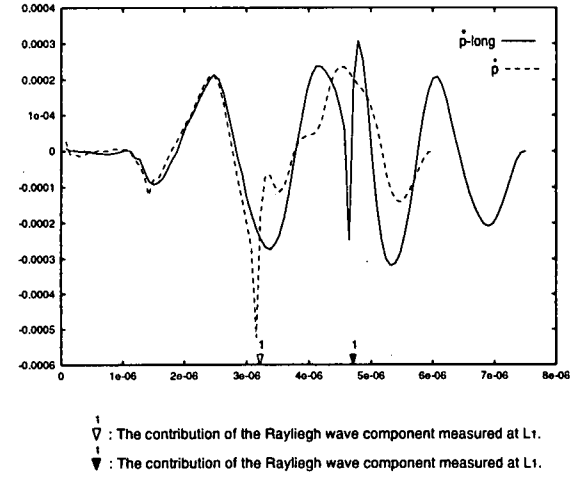

Fig. 5 Reconstructed pressure rate $\dot{p}$. $\dot{p}$: reconstructed pressure rate using data in the interval $(0, T)$, $\dot{p}$-long: reconstructed pressure rate using data in the interval $(0, T + \Delta T)$

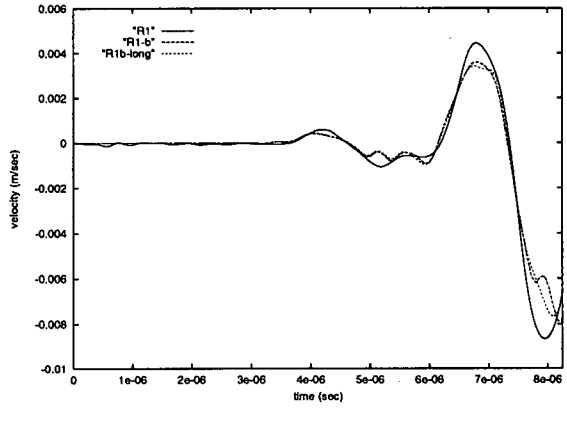

Fig. 6 Computed and measured normal velocity at R_1. R_1: measured, R_1-b: computed, R_1b-long: computed using $\dot{p}$ in the longer interval

velocity at R_1 observed experimentally (R_1), with the one computed with the method in Yoshikawa et al.[3] (R_1b) which is expected to be contaminated, and another computed with the elongated experimental data (R_1b-long) and the 2-DOF approximation for $\dot{p}$. The anomalous behaviour near $t = 8(\mu s)$ is seen to disappear in the result obtained with the elongated experimental data. From this result the use of elongated

experimental data is seen to be effective for improving the quality of the inversion result. It is also observed, however, that this technique alone may not necessarily be sufficient for the use of this inversion result in the second inverse problem of determining defects. This is because one still sees some difference between observed and computed results in Fig.6.

As an additional means to improve the quality of the inversion, we propose to take the observation points L_i closer to the transducer. In this way the Rayleigh waves from the transducer are observed at L_i for longer periods of time, thus increasing the information of $\dot{p}$ in the data. However, one has to be careful not to take these points too closely to each other since too close observation points will lead to degeneracy of the data.

With these considerations we shall test a new experimental setting in the next section. Namely, we shall combine the use of the elongated experimental data together with the use of observation points closer to the transducer than in the previous investigation.

4. New Experimental Setting

In the new experimental setting, we take 5 measuring points L_i $(i = 1, \ldots, 5)$ which are taken 2mm apart from each other. The location of L_1 is now 23mm away from the centre of the specimen, i.e., 1mm farther from the transducer than in the previous investigation. This undesired compromise is made in order to avoid possible contact between the transducer and the head of the laser interferometer. Also, the observation points R_{1-3} shown in Fig.7 are used to measure elastic waves affected by the cylindrical defect. Other details of the specimen are exactly the same as have been used in Yoshikawa et al.[3] and shown in Fig.1.

In the inversion to determine the elastic wave from the transducer, we set the equivalent load p_1 to be distributed on the circular area (∂D_{t_1}) having the radius of three fourths of the radius of the transducer, and the other (p_2) on the rest of the area (∂D_{t_2}) under the transducer, respectively.

For the determination of $\dot{p}_j$ for the interval of 6μs we use data in a longer measuring interval of 7.5μs. Then we discard the unreliable later part (for 1.5μs) and use $\dot{p}_j$ in the interval of $0 \leq t \leq 6(\mu s)$. Fig.8

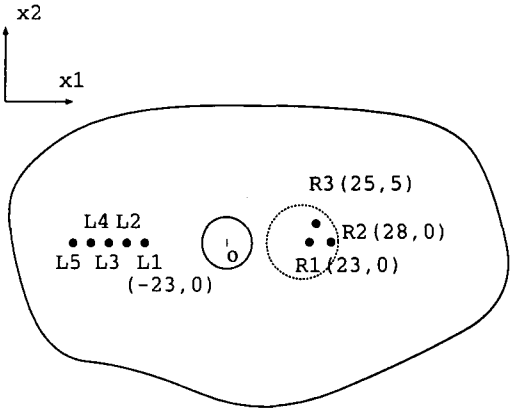

Fig. 7 The location of the measuring points.

shows the behaviour of $\dot{p}_j$ obtained as functions of time. In this figure the anomalous behaviour of $\dot{p}_j$ at the backward arrival time of the Rayleigh wave associated with L_1 is not visible, possibly reflecting the increased information of the data introduced by the change of the locations of the observation points. However a weak spiky behaviour associated with L_2 at $t \approx 3.7(\mu s)$ is seen.

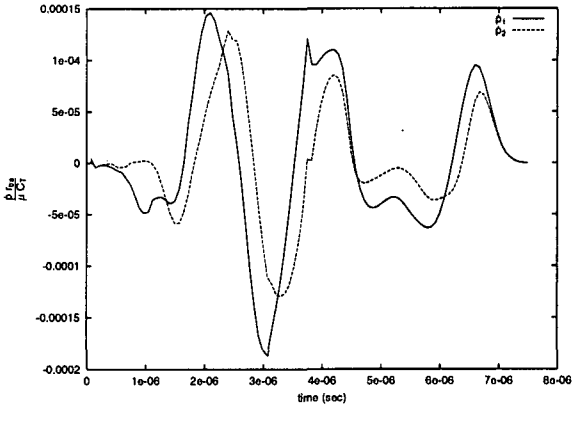

Fig. 8 Reconstructed pressure rates $\dot{p}_j$.

With $\dot{p}_i$ in the interval of $0 \leq t \leq 6(\mu s)$ thus obtained one may solve ordinary direct problem to compute the velocities at R_{1-3} numerically. In the present analysis we have used a 3 dimensional time domain BIEM with a truncated plane boundary to this end. The number of boundary elements used (N) are 4400, and the velocities of P and S waves are set equal to $c_L = 6400\text{m/s}$ and $c_T = 3100\text{m/s}$, respectively. The time increment Δt is 0.075 (μs), and the number of the time steps N_t is 110. Since the problem is fairly

large, we have parallelised the code using MPI[8]. The code was then run with 10 processors. Fig.9 shows the mesh used for the analysis. Fig.10 shows the normal

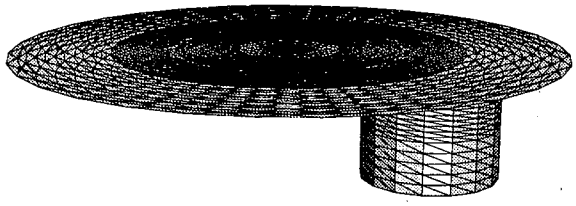

Fig. 9 Mesh.

velocities at R_{1-3} computed using the inversion results for $\dot{p}_j(t)$ and BIEM (marked R_i−b), and the corresponding experimental results (marked R_i). These results agree well.

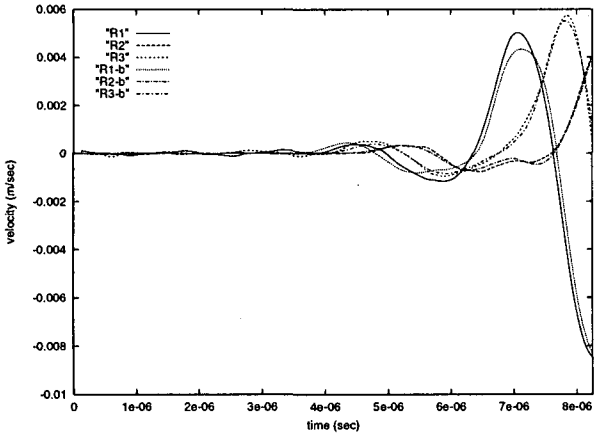

Fig. 10 Computed and observed velocities at R_{1-3}.

The smooth behaviour of $\dot{p}$ shown in Fig.8 suggests that the results in Fig.8 might be used to compute normal velocities beyond $t_0 + T$. This is done in Fig.11, which shows the computed normal velocity at R_1 obtained with the full data for $\dot{p}$ for $T = 7.5(\mu s)$ and BIEM (marked R_1-b) and the experimental data(marked R_1). The agreement between the experimental and computed results is quite remarkable. This result suggests that the new locations of the observation points are effective in improving the accuracy of the inversion results. Considering the effectiveness of the use of elongated experimental data concluded in the previous section, however, one may not be able to say only from this result that this observation point arrangement alone will be sufficient for the accurate determination of the elastic wave from the transducer.

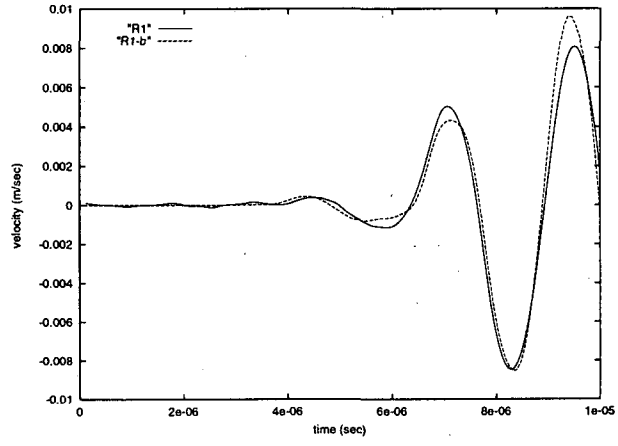

Fig. 11 Computed and observed velocities at R_1.

5. Determination of Defects

Encouraged by the agreement of the numerical and experimental results achieved in the previous section, we have tried to solve a simple inverse problem of determining the shape of an unknown defect from the real ultrasonic data obtained with the laser velocimetry. Namely, we have considered an inverse problem of estimating the depth and radius of the cylindrical defect from the velocity data at R_{1-3}, assuming that the other details of the geometry of the defects are known.

To solve this inverse problem, we introduce a cost function J defined by

$$J = \sum_{i=1}^{3} \sum_{m} (V^{R_i}(m\Delta t) - \boldsymbol{v}^{R_i}(r, d, m\Delta t) \cdot \boldsymbol{n})^2 \tag{7}$$

where V^{R_i} is the normal velocity obtained experimentally at the point R_i, and $\boldsymbol{v}^{R_i}(r, d, m\Delta t)$ stands for the velocity computed assuming that the radius and depth of the cylindrical defect are r and d, respectively. The most plausible defect is determined as the minimiser of this cost. The time increment Δt is $0.075(\mu s)$, and a time interval of about 6 (μs) is considered in the analysis.

Fig.12 gives a plot of the contour of the cost J. Instead of obtaining the minimum of J using non-linear programming techniques, we have evaluated J at the grid points in Fig.12, interpolated these values by a polynomial, and minimised J approximately by taking the minimum of the polynomial approximation of J. In this way we obtained $(r, d) = (9.506, 5.393)$(mm), the true values being $(r, d) = (9.9, 5.4)$(mm).

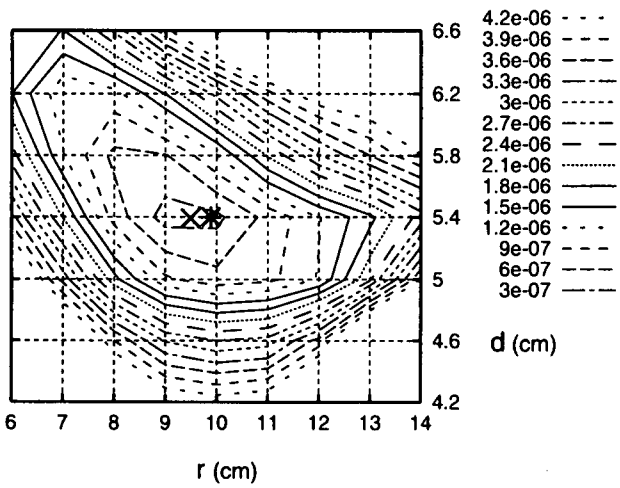

× : The solution of the inverse problem.

✳ : The true value.

Fig. 12 Contour of the cost.

6. Conclusion

With several improvements of the quality of the inversion proposed in this paper, we could verify that the reconstructed incident waves from the transducer are now quite reliable, and can be used in an inverse problem to determine an unknown defect. Indeed, in a simple problem, the size and location of an unknown defect could be determined with high accuracy from real data measured with a laser interferometer using the new experimental setting. Since our approach requires solutions of large scale problems using BIEM, however, we are still unable to solve more realistic defect determination problems. In the future work we therefore plan to use fast solution methods of BIEM such as FMBIEM (fast multipole BIEM) in order to complete the solution of defect determination problems using real data within a reasonable amount of time. Solutions of crack determination problems using real data are also of our interest.

REFERENCES

1) N. Nishimura and S. Kobayashi: Identification of transducer characteristics via BIEM and laser measurements, Proceedings of the 13th Japan National Symposium on Boundary Element Methods, pp.107–112, 1996. (in Japanese).
2) T. Kanbayashi, H. Yoshikawa, N. Nishimura and S. Kobayashi: Verification of ultrasonic transducer characteristics determined in an inverse problem based on laser measurements, *Inverse Problems in Engineering Mechanics II*,(Eds. M. Tanaka and G. S. Dulikravich), Elsevier, Amsterdam, pp.327–332, 2000.
3) H. Yoshikawa, N. Nishimura and S. Kobayashi: Identification of ultrasonic transducer characteristics for the determination of defects based on laser measurements and their verification with a parallel BIEM, Proceedings of the 17th Japan National Symposium on Boundary Element Methods, pp.59–64, 2000. (in Japanese).
4) N. Nishimura: Crack determination problems, *Theoretical and Applied Mechanics*, **46**, (Eds. G. Yagawa and C. Miki), Hokusensha Publ., Tokyo, pp.39–57, 1997.
5) A.N. Tikhonov and V.I. Arsenin: *Solution of Ill-Posed Problems*, Halsted Press, 1977.
6) C.A. Erigen and E.S. Suhubi: *Elastodynamics, Vol.II*, Academic Press, New York, 1975.
7) P.C. Hansen: Analysis of discrete ill-posed problems by means of the L-curve, *SIAM review* Vol.34, pp.561–580, 1992.
8) W. Gropp, E. Lusk and A. Skjellum, Using MPI: *Portable Parallel Programming with Message-Passing Interface*, second edition, MIT Press, Cambridge, Massachusetts, 1999.

(Received April 20, 2001)